

# The Inflationary Dynamics with the Scalar-Tensor Model

Feyzollah Younesizadeh and Davoud Kamani \*

*Department of Physics, Amirkabir University of Technology (Tehran Polytechnic)*

*P.O.Box: 15875-4413, Tehran, Iran*

*e-mails: fyounesizadeh@aut.ac.ir , kamani@aut.ac.ir*

## Abstract

We investigate the cosmic inflation within a class of the scalar-tensor model with the scalar-dependent non-minimal kinetic couplings. The inflationary dynamical potential will be applied. Using the slow-roll approximation, we compute theoretical predictions for the key observables, like the spectral indexes  $n_s$ , scalar-to-tensor ratio  $r$  and the running of the scalar spectral index  $\alpha_s$  in terms of the free parameters of the model. Besides, we find the limitations of these parameters. In addition, these quantities will be compared with the latest observational data from the Planck data. Furthermore, we analyze the sensitivity of  $r$ ,  $n_s$  and  $\alpha_s$  in terms of the model's free parameters.

*Keywords:* Scalar-tensor models; Running of spectral indexes; Inflationary dynamical potential; Slow-roll approximation; The Planck observational data.

---

\*Corresponding author

# 1 Introduction

The cosmological inflation explains the present large-scale structure. Besides, it addresses the important problems in the standard cosmology [1]-[8]. In extensive studies of the inflationary models, many theories of the gravity have been recently taken into consideration [9]-[36]. A major challenge in constructing the inflationary models is the flatness and stability of the inflaton potential against the quantum corrections to sustain the slow-roll inflation. The quantum fluctuations during the inflation act as the initial conditions for the large-scale structures and anisotropies [23]-[25].

We consider a special theoretical framework for investigating the inflation. It is called dynamical inflation (DI), that solves certain limitations inherent in the conventional inflationary models, including the adjusting of the inflation potential and the initial conditions for it [5]-[8], [37], [38].

In fact, the DI potential fails to achieve a successful transition out of the inflation and results in the spectral index  $n_s$  that exceeds the current observational thresholds. By incorporating further interactions, such as the non-minimal kinetic coupling, we can improve the limitations of this potential. Hence, the spectral index  $n_s$  can be adjusted to align with the most recent observational data [27]-[29], which also facilitates a graceful exit from the inflationary phase.

The primary motivation for this work is to construct a robust and well-motivated extension of the DI scenario that can successfully align with the modern cosmological data. While the standard DI framework is theoretically appealing, its failure to produce a scalar spectral index  $n_s$  within the Planck bounds and its challenges with a graceful exit from inflation [37], [38], necessitate a physical modification rather than an ad hoc adjustment of the potential. Therefore, we introduce a non-minimal kinetic coupling of the form  $J(\phi)G_{\mu\nu}\partial^\mu\phi\partial^\nu\phi$ . This choice is strongly motivated by a high-energy physics perspective. In fact, such couplings naturally arise in the low-energy effective action of the string theory and they are part of the healthy, the ghost-free Horndeski class of scalar-tensor theories [39], [40]. This provides a compelling and theoretically consistent avenue for modifying the inflationary dynamics.

This model offers some specific advantages relative to the standard slow-roll inflation in the general relativity (GR). Firstly, the coupling  $J(\phi)$  effectively flattens the scalar field potential during the inflation, not by fine-tuning  $V(\phi)$  itself but by modifying the kinetic energy of the inflaton. This naturally suppresses the tensor-to-scalar ratio  $r$  and it can significantly adjust the scalar spectral index  $n_s$ , pulling it into the observationally favored range. Secondly, this interaction can facilitate a graceful exit from the inflationary phase. The key limitation, common to many beyond-GR models, is the introduction of new functional degrees of freedom. Here, it is the functional  $J(\phi)$  with its parameters  $\alpha, \beta$  and  $\mu$ . Its possible naturalness issue at high energies is the largeness of  $J(\phi)$ . However, as we shall demonstrate, these parameters are not arbitrarily fine-tuned. In fact, they are constrained to specific natural ranges by the observational data, and their impact is physically interpretable through the model's sensitivity.

In this paper, we investigate the inflation via a modified gravity, which is characterized by the kinematically coupling term  $J(\phi)G_{\mu\nu}\partial^\mu\phi\partial^\nu\phi$ . We shall apply a special DI potential and an appropriate form for the functional  $J(\phi)$ , which includes some free parameters. Within the slow-roll approximation, we derive precise analytical expressions for the key physical quantities such as the scalar spectral index  $n_s$ , the tensor-to-scalar ratio  $r$  and the running of the scalar spectral index  $\alpha_s$ . According to the Planck data, we observe that this model leads to a more successful inflation than the standard DI model. Besides, we present sensitivity plots of the  $n_s$ ,  $r$  and  $\alpha_s$  in terms of the foregoing free parameters of the model.

This paper is organized as follows. In Sec. 2, we derive the equations of motion and the slow-roll parameters “ $n_s$ ”, “ $r$ ” and “ $\alpha_s$ ”. In Sec. 3, the DI via our model will be investigated. This provides a comparative analysis of our findings against the data from the Planck 2018. Finally, the section 4 is devoted to the results and conclusions.

## 2 The setup and field equations

We consider a generalized scalar-tensor model with a non-minimal kinetic coupling of the real scalar field  $\phi$  to the Einstein's tensor. In the Einstein frame, the corresponding

action can be written as,<sup>†</sup>

$$S = \int d^4x \sqrt{-g} \left( \frac{1}{2\kappa^2} R - \frac{1}{2} \partial_\mu \phi \partial^\mu \phi - V(\phi) + J(\phi) G_{\mu\nu} \partial^\mu \phi \partial^\nu \phi \right), \quad (2.1)$$

where  $G_{\mu\nu} = R_{\mu\nu} - \frac{1}{2} g_{\mu\nu} R$  is the Einstein's tensor. The functional  $J(\phi)$  is differentiable, and  $V(\phi)$  is the potential of the scalar field. For the derivations in this section, we work in units where  $M_P = 1$ . However, we shall restore it in the section 3 for consistency with observational data.

We assume a homogeneous scalar field  $\phi = \phi(t)$ , in a homogeneous and isotropic FRW background metric

$$ds^2 = -dt^2 + a(t)^2(dx^2 + dy^2 + dz^2). \quad (2.2)$$

Thus, the corresponding equations of motion find the following features

$$3H^2 = \frac{1}{2} \dot{\phi}^2 + V(\phi) + 9H^2 J(\phi) \dot{\phi}^2, \quad (2.3)$$

$$-2\dot{H} = \dot{\phi}^2 \left( 1 + 6H^2 J(\phi) \right) - 2 \frac{d}{dt} \left( H J(\phi) \dot{\phi}^2 \right), \quad (2.4)$$

$$\ddot{\phi} + 3H\dot{\phi} + V'(\phi) = -6HJ(\phi)\dot{\phi} \left( 3H^2 + 2\dot{H} \right) - 3H^2 \left( 2J(\phi)\ddot{\phi} + J'(\phi)\dot{\phi}^2 \right). \quad (2.5)$$

The Hubble parameter (function) is defined by  $H \equiv \dot{a}(t)/a(t)$ . For the special case  $J = 0$ , our model reduces to the standard Friedman equations with the single scalar field.

Through a straightforward calculation, we derive the following expressions for  $\dot{\phi}^2$  and  $V(\phi)$  from the foregoing field equations

$$V(\phi) = H^2 \left( 3 - \epsilon_1 - 2\ell_0 - \frac{1}{3} \ell_0 (\ell_1 - \epsilon_1) \right), \quad (2.6)$$

$$\dot{\phi}^2 = H^2 \left( 2\epsilon_1 - 2\ell_0 + \frac{2}{3} \ell_0 (\ell_1 - \epsilon_1) \right), \quad (2.7)$$

where the parameters, which are specifically characterized during the inflationary phase, are given by

$$\epsilon_1 = -\frac{\dot{H}}{H^2}, \quad \epsilon_2 = \eta = \frac{\dot{\epsilon}_1}{H\epsilon_1}, \quad \epsilon_3 = \frac{\dot{\epsilon}_2}{H\epsilon_2}, \quad \ell_0 = 3J(\phi)\dot{\phi}^2, \quad \ell_1 = \frac{\dot{\ell}_0}{H\ell_0}. \quad (2.8)$$

where  $\epsilon_1$  and  $\epsilon_2$  represent the Hubble flow parameters. In fact, one can employ the slow-roll approximation to effectively align the proposed model with the observational data.

---

<sup>†</sup>We use the natural units  $c = \hbar = 1$ ,  $\kappa^2 = M_p^{-2} = 8\pi G$ .

Hence, under the slow-roll conditions  $|\ddot{\phi}| \ll |3H\dot{\phi}|$  and  $\epsilon_1, \epsilon_2, \epsilon_3, \ell_0, \ell_1 \ll 1$ , Eqs. (2.3)-(2.5) take the forms

$$3H^2 - V(\phi) \simeq 0, \quad (2.9)$$

$$2\dot{H} + \dot{\phi}^2 \simeq -6H^2 J(\phi) \dot{\phi}^2 = -2\ell_0 H^2, \quad (2.10)$$

$$\dot{\phi} + \frac{V'(\phi)}{3H} \simeq -6H^2 J(\phi) \dot{\phi} = -\frac{2\ell_0 H^2}{\dot{\phi}}. \quad (2.11)$$

Using Eq. (2.8), we have  $\epsilon_1 \equiv \epsilon_V$  and  $\eta \approx -2\left(\frac{V''}{V} - 2\epsilon_V\right) = -2\eta_V + 4\epsilon_V$  [41]. The slow-roll analysis reveals the significant parameters as

$$\epsilon_V = \frac{1}{2(1 + 2V(\phi)J(\phi))} \left( \frac{V'(\phi)}{V(\phi)} \right)^2, \quad (2.12)$$

$$\begin{aligned} \eta_V = & - \frac{2}{(1 + 2V(\phi)J(\phi))} \frac{V''}{V} + \frac{3}{2(1 + 2V(\phi)J(\phi))} \left( \frac{V'(\phi)}{V(\phi)} \right)^2 J(\phi) \\ & + \frac{4}{(1 + 2V(\phi)J(\phi))^2} \left( \frac{V'(\phi)}{V(\phi)} \right) \left( J(\phi)V'(\phi) + V(\phi)J'(\phi) \right). \end{aligned} \quad (2.13)$$

Within the framework of the inflationary model scenarios, the scalar field value  $\phi_e$  at the end of the expansion is obtained through  $\epsilon_1(\phi_e) = 1$ . Besides, the scalar field at the commencement of the inflation can be determined by analyzing the total logarithmic phase. It is important to note that the number of e-folds, related to the inflationary period, is crucial for interpreting the cosmological observables. It is generally given by

$$N = \int_{t_i}^{t_e} H dt = \int_{\phi_i}^{\phi_e} \frac{H}{\dot{\phi}} d\phi = - \int_{\phi_i}^{\phi_e} \left( \frac{3H^2 + 18H^4 J(\phi)}{V'(\phi)} \right) d\phi. \quad (2.14)$$

In super-horizon scale ( $k \ll aH$ ), the power spectra of the scalar perturbations demonstrate the following  $k$ -dependence

$$P_\zeta = \frac{k^3}{2\pi^2} |\zeta_k|^2 \propto k^{3-2\mu_s}, \quad (2.15)$$

where in the mentioned model, the range of the scalar disturbances is

$$\zeta_k \propto k^{-\mu_s}, \quad \mu_s = \epsilon_1 + \frac{1}{2}\eta + \frac{3}{2}. \quad (2.16)$$

Here,  $\zeta_k$  denotes the curvature perturbation mode. Therefore, the scalar spectral index becomes

$$n_s = 1 + \frac{d \ln P_\zeta}{d \ln k} = 4 - 2\mu_s = 1 - 2 \left( \epsilon_1 + \frac{1}{2}\eta \right) = 1 - 6\epsilon_V + 2\eta_V. \quad (2.17)$$

The slow-roll parameter  $\ell_0$ , which pertains to the kinetic coupling, does not appear in the scalar spectral index.

An essential quantity is the relative contribution of the tensor and scalar perturbations to the power spectra. It is defined via the tensor-to-scalar ratio  $r$ ,

$$r = \frac{P_T(k)}{P_\zeta(k)}. \quad (2.18)$$

By applying Eq. (2.15), the power spectra for the scalar perturbations is

$$P_\zeta = \frac{H^2 A_S}{4\pi^2} \frac{\left[ 3(1 - J(\phi)\dot{\phi}^2) + \frac{3}{V(\phi)} \left( \frac{1}{2}\dot{\phi}^2 - V(\phi) + 6V(\phi)J(\phi)\dot{\phi}^2 \right) \left( \frac{1 - J(\phi)\dot{\phi}^2}{1 - 3J(\phi)\dot{\phi}^2} \right)^2 \right]^{1/2}}{\left[ \frac{1}{a} \frac{d}{dt} \left( \frac{3\dot{a}}{V(\phi)} \frac{(1 - J(\phi)\dot{\phi}^2)^2}{1 - 3J(\phi)\dot{\phi}^2} \right) - (1 + J(\phi)\dot{\phi}^2) \right]^{3/2}}, \quad (2.19)$$

where Eq. (2.19) has been derived in [32], in which the perturbations for the non-minimal kinetic couplings have been computed by using the Sasaki-Mukhanov variable. Also, the parameter  $A_S$  is defined as follows

$$A_S = 4^{\mu_s - 2} \left| \frac{\Gamma(\mu_s)}{\Gamma(3/2)} \right|^2. \quad (2.20)$$

The evaluation of all magnitudes occurs at the moment of the horizon exit, in which  $k = aH$ . Analogously, the power spectra for the tensor perturbations have the feature [32],

$$P_T = 16 \frac{H^2 A_T}{4\pi^2} \frac{\left[ 1 - J(\phi)\dot{\phi}^2 \right]^{1/2}}{\left[ 1 + J(\phi)\dot{\phi}^2 \right]^{3/2}}, \quad (2.21)$$

$$A_T = 4^{\mu_T - 2} \left| \frac{\Gamma(\mu_T)}{\Gamma(3/2)} \right|^2. \quad (2.22)$$

In the limit  $\epsilon_1, \epsilon_2, \epsilon_3, \ell_0, \ell_1 \ll 1$ , and using  $\mu_s = \epsilon_1 + \frac{1}{2}\eta + \frac{3}{2}$  and  $\mu_T = \epsilon_1 + \frac{3}{2}$ , we obtain  $A_T = A_S$ . By considering the  $P_\zeta$  and  $P_T$  in Eqs. (2.19) and (2.21), up to the first order, and using the condition  $\epsilon_1, \epsilon_2, \epsilon_3, \ell_0, \ell_1 \ll 1$ , the parameter  $r$  is approximately given by

$$r = 16\epsilon. \quad (2.23)$$

In order to compare the results with the experimental data, one can also investigate the running of the scalar spectral index  $\alpha_s$ , which is defined as

$$\alpha_s = \frac{dn_s}{d \ln k} = \frac{d^2 \ln P_\zeta}{d \ln k^2}, \quad (2.24)$$

where  $d/d \ln k = -d/dN$  [42]. According to the Planck 2018 data, the parameters of the cosmic disturbances must meet the following observational limitations [27]-[29],

$$n_s = 0.9663 \pm 0.0041, \quad r < 0.065, \quad \alpha_s = -0.0041 \pm 0.0067, \quad (2.25)$$

with 68% C.L and 95% C.L, respectively.

### 3 The dynamical inflation

The DI represents a distinct class of inflationary models that emerge in the early universe. This framework employs dynamic processes, including non-linear field dynamics, phase transitions, and moduli stabilization, to drive inflation. Such models specifically aim to overcome limitations of conventional inflationary scenarios by stabilizing scalar fields (potential inflaton candidates) and utilizing dynamical mechanisms to produce an appropriately flat potential [37]-[42].

The DI relies on the dynamical mechanisms to generate the inflationary potential. These mechanisms often involve the non-perturbative effects, such as the gaugino condensation or the moduli stabilization in the string theory, which naturally give rise to some flat potentials suitable for inflation. An appropriate DI potential is [38],

$$V(\phi) = V_0 \left[ 1 + \left( \frac{\phi}{\mu} \right)^{-p} \right], \quad (3.1)$$

$$V_0 = M^4, \quad \mu^p = \frac{\Lambda_3^{p+4}}{M^4}, \quad (3.2)$$

where “ $p$ ” is a free parameter, and the scale of  $\Lambda_3$  is determined by the associated gauge group.

We apply the DI potential (3.1), and we also consider the following non-minimum kinetic coupling  $J(\phi)$ ,

$$J(\phi) = \frac{1}{J_0} \left[ \alpha + \beta \left( \frac{\phi}{\mu} \right)^{-p} \right], \quad (3.3)$$

here we assume that  $V_0 = J_0$ , and also  $\alpha$  and  $\beta$  are arbitrary parameters. In the action (2.1), if  $J(\phi) = 0$  we can obtain the slow-roll parameters. Thus, the spectral index  $n_s$  can be articulated through the slow-roll parameters as

$$n_s = 1 - 2\epsilon_1 - \eta = 1 - 6\epsilon_V + 2\eta_V. \quad (3.4)$$

The running of the scalar spectral index is given by [41],[42],

$$\alpha_s = -2\xi^2 - 8\epsilon_V^2 + 10\epsilon_V\eta_V, \quad (3.5)$$

The higher-order slow-roll parameter  $\xi^2$ , which contributes to the running  $\alpha_s$ , is defined as

$$\begin{aligned} \xi^2 &\equiv \frac{M_{\text{Pl}}^4}{16\pi^2} \frac{H'(\phi)H'''(\phi)}{H^2(\phi)} \\ &\simeq \frac{M_{\text{Pl}}^4}{64\pi^2} \left[ \frac{V'(\phi)V'''(\phi)}{V^2(\phi)} - \frac{3}{2} \left( \frac{V'(\phi)}{V(\phi)} \right)^2 \frac{V''(\phi)}{V(\phi)} + \frac{3}{4} \left( \frac{V''(\phi)}{V(\phi)} \right)^4 \right]. \end{aligned} \quad (3.6)$$

This is another parameter, associated with the slow-roll dynamics. By utilizing (2.23), the Eq. (3.5) can be approximately rewritten as

$$\alpha_s \simeq 0.12r^2 - 0.57r(1 - n_s) - \frac{M_{\text{Pl}}^4}{32\pi^2} \frac{V'(\phi)V'''(\phi)}{V^2(\phi)}. \quad (3.7)$$

In fact, the last term in this equation is paramount in DI models.

The first slow-roll parameter is given by

$$\epsilon_V(\phi) = \frac{M_{\text{Pl}}^2}{2} \left( \frac{V'(\phi)}{V(\phi)} \right)^2 = \frac{p^2 M_{\text{Pl}}^2}{2\mu^2} \frac{\left( \frac{\mu}{\phi} \right)^{2p+2}}{\left[ 1 + \left( \frac{\mu}{\phi} \right)^p \right]^2}. \quad (3.8)$$

At the end of the inflation there is  $\epsilon_V(\phi_{\text{end}}) \approx 1$ . Thus, we receive the following algebraic equation for the value of the inflaton for terminating the inflation

$$\frac{pM_{\text{Pl}}}{4\mu} \left( \frac{\mu}{\phi_{\text{end}}} \right)^{p+1} - \left( \frac{\mu}{\phi_{\text{end}}} \right)^p - 1 = 0. \quad (3.9)$$

For  $p = 1$ , the inflaton  $\phi_{\text{end}}$  explicitly finds the value

$$\phi_{\text{end}} = \frac{M_{\text{Pl}}}{2 \left( 1 + \sqrt{1 + M_{\text{Pl}}/\mu} \right)}. \quad (3.10)$$

If  $\mu \gg M_{\text{Pl}}$ , this obviously reduces to  $\phi_{\text{end}} \approx M_{\text{Pl}}/4$ . For general value of  $p$  and also the case  $\phi_{\text{end}} \ll \mu$ , the denominator of Eq. (3.8) tends to  $(\mu/\phi)^{2p}$  (or equivalently the third term of Eq. (3.9) becomes negligible). Hence, Eq. (3.9) possesses the solution

$$\phi_{\text{end}} \approx \frac{pM_{\text{Pl}}}{4}. \quad (3.11)$$

This value of the inflaton is independent of the parameter  $\mu$ , while it is proportional to the Planck mass. Note that the condition  $\phi_{\text{end}} \ll \mu$  clearly defines large value for the parameter  $\mu$ , i.e.,  $\mu \gg \frac{p}{4}M_{\text{Pl}}$ .

If  $\phi_{\text{end}} \gg \mu$ , the denominator of Eq. (3.8) tends to 1 (or equivalently the second term of Eq. (3.9) becomes negligible). In this case, the reduced form of Eq. (3.9) gives

$$\phi_{\text{end}} \approx \left( \frac{p\mu^p M_{\text{Pl}}}{4} \right)^{\frac{1}{p+1}}. \quad (3.12)$$

Hence, the inequality  $\phi_{\text{end}} \gg \mu$  finds the feature  $\mu \ll pM_{\text{Pl}}/4$ . Now we transform the parameter  $\mu$  to another parameter  $\gamma$ , i.e.,  $\mu = \gamma M_{\text{Pl}}$ . Thus,, the above  $\phi_{\text{end}}$  takes the form

$$\phi_{\text{end}} \approx \left( \frac{p\gamma^p}{4} \right)^{\frac{1}{p+1}} M_{\text{Pl}}. \quad (3.13)$$

Therefore, the inequality  $\phi_{\text{end}} \gg \mu$  imposes the following condition on the parameter  $\gamma$ , i.e.,  $\gamma \ll p/4$ .

We observe that by adjusting the parameters we receive various values for  $\phi_{\text{end}}$ , which are proportional to the Planck mass  $M_{\text{Pl}}$ . This result prominently is consistent with the literature [27], [43]-[49].

The second slow-roll parameter is

$$\eta_{\text{V}}(\phi) = \epsilon_{\text{V}} - \frac{M_{\text{Pl}}}{4\sqrt{\pi}} \frac{\epsilon'_{\text{V}}}{\sqrt{\epsilon_{\text{V}}}} = \left( \frac{\phi_0}{\phi} \right)^{2(p+1)} + \frac{p+1}{2\sqrt{\pi}} \frac{M_{\text{Pl}}}{\phi} \left( \frac{\phi_0}{\phi} \right)^{p+1}, \quad (3.14)$$

where  $\phi_0 = M_{\text{Pl}} \left( \frac{p}{4\sqrt{\pi}} \lambda \right)^{1/(p+1)}$ . In the case  $\lambda \ll (\phi/M_{\text{Pl}})^p$ , with  $\lambda = (\mu/M_{\text{Pl}})^p$ , the constant  $V_0$  in Eq. (3.1) plays a dominant role in the potential.

It is crucial to note that when  $\phi \simeq \phi_0 \ll M_{\text{Pl}}$ , the parameter  $\eta_{\text{V}}$  becomes very large and  $\epsilon_{\text{V}}(\phi) \simeq 1$ , which suggest a breakdown of the slow-roll approximation. In other words, it is inconsistent to the state that the inflation initiates at  $\phi = \phi_0$ . For the second case

$\phi \gg \phi_0$ , both  $\epsilon_V$  and  $\eta_V$  become small, which admits a consistent slow-roll approximation. In the third case  $\phi_0 \ll \phi \ll M_{\text{Pl}}$ , the second term of (3.14) becomes the dominant factor, which leads to the condition  $\eta_V \gg \epsilon_V$ . Thus,  $\eta$  can be reformulated as in the following

$$\eta_V(\phi) \simeq \frac{p+1}{2\sqrt{\pi}} \sqrt{\epsilon_V(\phi)} \frac{M_{\text{Pl}}}{\phi} = \frac{\lambda p(p+1)}{8\pi} \left( \frac{M_{\text{Pl}}}{\phi} \right)^{p+2}. \quad (3.15)$$

The number of e-folds can be expressed as

$$N = \frac{2\sqrt{\pi}}{M_{\text{Pl}}} \int_{\phi}^{\phi_c} \frac{d\phi'}{\sqrt{\epsilon_V(\phi')}} \simeq \frac{p+1}{p+2} \left( \frac{1}{\eta_V(\phi_c)} - \frac{1}{\eta_V(\phi)} \right), \quad \epsilon_V \ll \eta_V. \quad (3.16)$$

The field value  $\phi_c$  refers to the critical point in which inflation has ceased. We shall consider  $\phi_c$  as a free parameter. However, combining Eqs. (3.15) and (3.16), and also imposing  $\phi \ll \phi_c$ , the number of e-folds  $N$  tends to the following constant value

$$N_{\text{tot}} \equiv \frac{p+1}{p+2} \frac{1}{\eta_V(\phi_c)} = \frac{8\pi}{\lambda p(p+2)} \left( \frac{\phi_c}{M_{\text{Pl}}} \right)^{p+2}. \quad (3.17)$$

This upper limit can be very large. By defining  $\phi_N$  as the field value at the  $N$  e-folds before inflation, we can articulate  $\eta_V(\phi_N)$  in terms of  $N$  and  $N_{\text{tot}}$ ,

$$\eta_V(\phi_N) = \frac{p+1}{p+2} \frac{1}{N_{\text{tot}} - N}. \quad (3.18)$$

Consequently, when  $N \ll N_{\text{tot}}$ ,  $\eta_V$  approaches to a constant value. The spectral index can be written as

$$n_s = 1 + 2\eta_V - 6\epsilon_V \simeq 1 + \frac{p+1}{p+2} \frac{2}{N_{\text{tot}}} \left( 1 - \frac{50}{N_{\text{tot}}} \right)^{-1}. \quad (3.19)$$

Thus, the running of the scalar spectral index can be represented as a function of the spectral index

$$\alpha_s = -\frac{1}{2} \frac{p+2}{p+1} (n_s - 1)^2. \quad (3.20)$$

In the special case where  $J(\phi) = 0$ , the values for  $n_s$  and  $r$  approximately fall within the ranges  $n_s \in [1, 1.06]$  and  $r \in [10^{-14}, 10^{-7}]$  for  $p = 2$ ;  $n_s \in [1, 1.06]$  and  $r \in [10^{-17}, 10^{-6}]$  for  $p = 3$ ; and  $n_s \in [1, 1.06]$  and  $r \in [10^{-20}, 10^{-4}]$  for  $p = 4$ . The values of  $r$  precisely are consistent with the Planck data, while the values of  $n_s$  do not align with the same dataset [50].

Now consider the case where  $J(\phi)$  takes the form of (3.3). Thus, the slow-roll parameters and the other related factors are modified. In order to calculate  $n_s$  and  $r$ , it is useful to employ the parameters  $\epsilon_V$  and  $\eta_V$ . They can be represented as follows

$$\epsilon_V = \frac{1}{4} \frac{p^2 \left(\frac{\phi}{\mu}\right)^{-2p}}{\phi^2 \left(1 + \left(\frac{\phi}{\mu}\right)^{-p}\right)^2 \left[ \beta \left(\frac{\phi}{\mu}\right)^{-2p} + (\beta + \alpha) \left(\frac{\phi}{\mu}\right)^{-p} + \alpha + \frac{1}{2} \right]}, \quad (3.21)$$

$$\begin{aligned} \eta_V &= \frac{7 \left[ \beta \left(\frac{\phi}{\mu}\right)^{-2p} + (\beta + \alpha) \left(\frac{\phi}{\mu}\right)^{-p} + \alpha + \frac{1}{2} \right]^{-2}}{4\phi^2 \left(1 + \left(\frac{\phi}{\mu}\right)^{-p}\right)^2} \\ &\times \left\{ p \left(\frac{\phi}{\mu}\right)^{-p} \left[ \beta \left(p - \frac{4}{7}\right) \left(\frac{\phi}{\mu}\right)^{-3p} + \left( \alpha \left(\frac{3}{7}p - \frac{4}{7}\right) + \beta \left(p - \frac{8}{7}\right) \right) \left(\frac{\phi}{\mu}\right)^{-2p} \right. \right. \\ &\left. \left. + \left( \alpha \left(-\frac{p}{7} - \frac{8}{7}\right) - \frac{p}{14} - \frac{4}{7}\beta - \frac{2}{7} \right) \left(\frac{\phi}{\mu}\right)^{-p} - \frac{4}{7} \left(\alpha + \frac{1}{2}\right) (p + 1) \right] \right\}. \quad (3.22) \end{aligned}$$

The number of e-folds has the form

$$\begin{aligned} N &= \frac{\phi^2}{p(p-1)(p-2)(p+2) \left(\frac{\phi}{\mu}\right)^{-p}} \left\{ \left( -\beta p^2 + 4\beta \right) \left(\frac{\phi}{\mu}\right)^{-3p} \right. \\ &- 4(p-1)(p+2) \left(\frac{1}{2}\alpha + \beta\right) \left(\frac{\phi}{\mu}\right)^{-2p} + (p-1)(p-2)(p+2) \left(\beta + 2\alpha + \frac{1}{2}\right) \left(\frac{\phi}{\mu}\right)^{-p} \\ &\left. + 2(p-1)(p-2) \left(\alpha + \frac{1}{2}\right) \right\}. \quad (3.23) \end{aligned}$$

To obtain the observables as functions of  $N$ , we numerically invert Eq. (3.23) for  $\phi(N)$  and substitute into Eqs. (3.20)-(3.22). This is done for each parameter set, which ensures consistency with the slow-roll approximation. In the same way, both the tensor-to-scalar ratio and the spectral index takes the features

$$r = \frac{8p^2 \left(\frac{\phi}{\mu}\right)^{-2p}}{\phi^2 \left(1 + \left(\frac{\phi}{\mu}\right)^{-p}\right)^2 \left[ 1 + 2 \left(1 + \left(\frac{\phi}{\mu}\right)^{-p}\right) \left(\alpha + \beta \left(\frac{\phi}{\mu}\right)^{-p}\right) \right]}, \quad (3.24)$$

$$\begin{aligned}
n_s &= 1 + \frac{1}{\phi^2 \left(1 + \left(\frac{\phi}{\mu}\right)^{-p}\right) \left[\beta \left(\frac{\phi}{\mu}\right)^{-2p} + (\beta + \alpha) \left(\frac{\phi}{\mu}\right)^{-p} + \alpha + \frac{1}{2}\right]} \\
&\times \left\{ p(p+1) \left(\frac{\phi}{\mu}\right)^{-p} - \frac{p^2 \left(2\beta \left(\frac{\phi}{\mu}\right)^{-p} + \beta + \alpha\right) \left(\frac{\phi}{\mu}\right)^{-2p}}{\beta \left(\frac{\phi}{\mu}\right)^{-2p} + (\beta + \alpha) \left(\frac{\phi}{\mu}\right)^{-p} + \alpha + \frac{1}{2}} \right. \\
&\left. - \frac{5}{4} \frac{p^2 \left(\frac{\phi}{\mu}\right)^{-2p}}{\left(1 + \left(\frac{\phi}{\mu}\right)^{-p}\right)} \right\}. \tag{3.25}
\end{aligned}$$

The running spectral index also finds the form

$$\begin{aligned}
\alpha_s &= -\frac{9}{4\phi^4 \left(1 + \left(\frac{\phi}{\mu}\right)^{-p}\right)^4 \left[\beta \left(\frac{\phi}{\mu}\right)^{-2p} + (\beta + \alpha) \left(\frac{\phi}{\mu}\right)^{-p} + \frac{1}{2} + \alpha\right]^4} \\
&\times \left\{ p^2 \left(\frac{\phi}{\mu}\right)^{-2p} \left\{ \left[\beta^2 (p-1) \left(p - \frac{4}{9}\right) \left(\frac{\phi}{\mu}\right)^{-6p}\right. \right. \right. \\
&+ \frac{3}{2}\beta \left(\left(\beta + \frac{5}{9}\alpha\right)p^2 + \left(-\frac{26\beta}{9} - \frac{40\alpha}{27}\right)p + \frac{32\beta}{27} + \frac{16\alpha}{27}\right) \left(\frac{\phi}{\mu}\right)^{-5p} \\
&+ \left(\left(-\frac{13\alpha\beta}{18} + \frac{5\alpha^2}{18} - \frac{7\beta}{18}\right)p^2 + \left(-6\alpha\beta - \frac{7\alpha^2}{9} - \frac{13}{3}\beta^2 - \frac{7\beta}{9}\right)p \right. \\
&+ \left.\left.\left.\left.\frac{4}{9}\alpha^2 + \frac{8}{3}\beta^2 + \frac{4}{9}\beta + \frac{32\alpha\beta}{9}\right) \left(\frac{\phi}{\mu}\right)^{-4p}\right] \right. \right. \\
&+ \left[\left(-\frac{4}{9}\alpha^2 + \left(-\frac{25\beta}{6} - \frac{1}{12}\right)\alpha - \frac{1}{2}\beta^2 - \frac{61\beta}{36}\right)p^2 \right. \\
&+ \left.\left(-\frac{5}{3}\alpha^2 + \left(-\frac{14}{3}\beta - \frac{4}{9}\right)\alpha - \frac{13\beta^2}{9} - \frac{11\beta}{9}\right)p + \frac{16\alpha^2}{9} + \left(\frac{4}{9} + \frac{16}{3}\beta\right)\alpha \right. \\
&+ \left.\left.\frac{16\beta^2}{9} + \frac{4}{3}\beta\right] \left(\frac{\phi}{\mu}\right)^{-3p} + \left[-\frac{17}{6}\left(\frac{1}{2} + \alpha\right)\left(\frac{9}{17}\alpha + \beta\right)p^2 \right. \right. \\
&- \left.\left.\frac{2}{9}\left(\frac{3}{2}\alpha + \beta + \frac{1}{4}\right)\left(\frac{1}{2} + \alpha\right)p + \frac{8}{3}\alpha^2 + \left(\frac{4}{3} + \frac{32\beta}{9}\right)\alpha \right. \right. \\
&+ \left.\left.\frac{1}{9} + \frac{4}{3}\beta + \frac{4}{9}\beta^2\right] \left(\frac{\phi}{\mu}\right)^{-2p} - \frac{2}{9}\left[\left(\beta + \frac{5}{2}\alpha + \frac{3}{4}\right)p - 4\beta \right. \right. \\
&\left. \left. - 8\alpha - 2\right] (p+1) \left(\frac{1}{2} + \alpha\right) \left(\frac{\phi}{\mu}\right)^{-p} + \frac{2}{9}(p+1)(p+2) \left(\frac{1}{2} + \alpha\right)^2 \right\} \Bigg\}. \tag{3.26}
\end{aligned}$$

By calculating the parameters  $r$ ,  $n_s$  and  $\alpha_s$ , and selecting the values for the free parameters  $\mu$ ,  $\alpha$  and  $\beta$  within a specific range, we can compare the outcomes of this

model against the data provided by the Planck 2018. Taking  $\alpha = \beta = 0$ , these quantities reduce to the standard gravity model with the coupling constant  $\kappa$ , as expected [51], [52].

In the Tables 1–3, by assigning specific values to the free parameters, we obtained results for the significant parameters (slow-roll parameters) of our model, namely  $r$  and  $n_s$ , together with the running of the spectral index  $\alpha_s$ . These results are entirely consistent with the Planck data. In contrast, for the case  $J(\phi) = 0$ , as previously discussed, the results do not correspond closely with the Planck data, except for the parameter  $r$ .

Table 1: The numerical calculations for the tensor-to-scalar ratio  $r$ , scalar spectral index  $n_s$ , and the running spectral index  $\alpha_s$  have been performed over  $N = 50 \rightarrow 60$  e-folds, via the parameters  $\alpha = -0.02$ ,  $\beta = 10$ ,  $p = 3$ , and different values of  $\mu$ .

$N$	$\mu$	$n_s$	$r$	$\alpha_s$
50 $\rightarrow$ 60	2.0	0.9627 $\rightarrow$ 0.9485	$15 \times 10^{-4} \rightarrow 2.0 \times 10^{-3}$	-0.00101 $\rightarrow$ -0.00197
50 $\rightarrow$ 60	2.1	0.9700 $\rightarrow$ 0.9615	$12 \times 10^{-4} \rightarrow 1.6 \times 10^{-3}$	-0.00065 $\rightarrow$ -0.00109
50 $\rightarrow$ 60	2.2	0.9750 $\rightarrow$ 0.9695	$10 \times 10^{-4} \rightarrow 1.2 \times 10^{-3}$	-0.00044 $\rightarrow$ -0.00067
50 $\rightarrow$ 60	2.3	0.9788 $\rightarrow$ 0.9749	$8.0 \times 10^{-4} \rightarrow 1.0 \times 10^{-3}$	-0.00032 $\rightarrow$ -0.00045
50 $\rightarrow$ 60	2.4	0.9817 $\rightarrow$ 0.9789	$7.0 \times 10^{-4} \rightarrow 8.0 \times 10^{-4}$	-0.00024 $\rightarrow$ -0.00032

After comparing the results in these tables for  $r$ ,  $n_s$  and  $\alpha_s$  with Eq. (2.25), we observe that the results are in excellent agreement with the Planck 2018 data.

It is clear that the parameters  $\alpha$ ,  $\beta$  and  $\mu$  must be fixed within a specific range. Hence, we do not have freedom to choose any values for them. Therefore, this is a very good result that our free parameters must be in a very specific range to be consistent with the Planck data. These results, which are stated in the above tables, have been plotted in the Figures 1–3.

In the Figure 1, we have shown the results from the data in the table 1. In this case,  $\alpha$  and  $\beta$  have specific fixed values, while  $\mu$  is variable, which changes in the interval  $\mu \in [2, 2.4]$ . It can be seen that the results of the  $n_s - r$  curve are in good agreement with the Planck data. Thus, we can claim that our model covers a large part of the experimental data, i.e., the Planck 2018 and BICEP/Keck dataset along with the recently released CMB-S4, and Stage 3 [53], [54]. It follows from the Figure 1 that  $r$  decreases with increasing  $\mu$  and fixing  $\alpha$  and  $\beta$ . By taking large values of  $\mu$ , the value of  $n_s$  decreases, and also  $n_s$  increases with increasing  $\mu$ .

### 3.1 Comparison with the recent ACT and CMB-S4 results

The Atacama Cosmology Telescope (ACT) DR6 [55], [56] data and the latest CMB-S4 forecasts further restrict the tensor-to-scalar ratio to  $r < 0.035$  (95 % C.L.) and slightly

Table 2: The numerical calculations for the tensor-to-scalar ratio  $r$ , scalar spectral index  $n_s$ , and the running spectral index  $\alpha_s$  have been performed over  $N = 50 \rightarrow 60$  e-folds, via the parameters  $\mu = 2$ ,  $\beta = 10$ ,  $p = 3$ , and different values of  $\alpha$

$N$	$\alpha$	$n_s$	$r$	$\alpha_s$
50 $\rightarrow$ 60	-0.07	0.9659 $\rightarrow$ 0.9543	$12.9 \times 10^{-4} \rightarrow 1.7 \times 10^{-3}$	-0.00085 $\rightarrow$ -0.00155
50 $\rightarrow$ 60	-0.09	0.9672 $\rightarrow$ 0.9566	$11.8 \times 10^{-4} \rightarrow 1.6 \times 10^{-3}$	-0.00079 $\rightarrow$ -0.00140
50 $\rightarrow$ 60	-0.11	0.9685 $\rightarrow$ 0.9589	$10.8 \times 10^{-4} \rightarrow 1.4 \times 10^{-3}$	-0.00072 $\rightarrow$ -0.00125
50 $\rightarrow$ 60	-0.13	0.9698 $\rightarrow$ 0.9611	$9.0 \times 10^{-4} \rightarrow 1.2 \times 10^{-3}$	-0.00066 $\rightarrow$ -0.00112
50 $\rightarrow$ 60	-0.15	0.9712 $\rightarrow$ 0.9634	$8.0 \times 10^{-4} \rightarrow 1.1 \times 10^{-3}$	-0.00060 $\rightarrow$ -0.00099
50 $\rightarrow$ 60	-0.17	0.9725 $\rightarrow$ 0.9656	$7.9 \times 10^{-4} \rightarrow 1.0 \times 10^{-3}$	-0.00055 $\rightarrow$ -0.00088
50 $\rightarrow$ 60	-0.19	0.9739 $\rightarrow$ 0.9677	$7.1 \times 10^{-4} \rightarrow 0.8 \times 10^{-3}$	-0.00049 $\rightarrow$ -0.00077
50 $\rightarrow$ 60	-0.21	0.9753 $\rightarrow$ 0.9699	$6.0 \times 10^{-4} \rightarrow 0.7 \times 10^{-3}$	-0.00044 $\rightarrow$ -0.00067

tighten the bounds on  $n_s = 0.9655 \pm 0.0035$ . The predictions of our model for  $r \sim 10^{-3}$ – $10^{-2}$  and  $n_s \simeq 0.95$ – $0.98$  remain well within these new limits. We have checked that the running  $\alpha_s$  stays in the range  $|\alpha_s| < 10^{-3}$ , which is compatible with both ACT and Planck results. Finally, we also compared our results with the latest ACT DR6 data, which agrees well with Planck data, and provides deeper primary CMB measurements. Our parameter ranges satisfy the updated constraints, which confirm the model’s viability.

Next, we analyze the Table 2. Its results have been plotted in the Figure 2. Here, we consider the parameters  $\mu$  and  $\beta$  to be fixed and the parameter  $\alpha$  as a variable which changes in the interval  $\alpha \in [-0.21, -0.07]$ . We observe that the results of the curve  $n_s - r$  are in agreement with the Planck data. By changing just one of the above parameters, we can cover a large portion of the data of the Planck satellite, CMB-S4 and Stage 3. For the Figure 2, the value of  $r$  decreases with decreasing  $\alpha$  and fixing  $\beta$  and  $\mu$ . By taking small values for  $\alpha$ , the range of  $n_s$  decreases, and  $n_s$  increases with decreasing  $\alpha$ .

Finally, the results of our analysis of the Table 3 have been shown in the Figure 3. Here, we assumed that  $\alpha$  and  $\mu$  are fixed, while  $\beta$  is a variable, which changes in the

Table 3: The numerical calculations for the tensor-to-scalar ratio  $r$ , scalar spectral index  $n_s$ , and the running spectral index  $\alpha_s$  have been performed over  $N = 50 \rightarrow 60$  e-folds, via the parameters  $\alpha = -0.02$ ,  $\mu = 2$ ,  $p = 3$ , and different values of  $\beta$ .

$N$	$\beta$	$n_s$	$r$	$\alpha_s$
50 $\rightarrow$ 60	10.4	0.9671 $\rightarrow$ 0.9566	$13.0 \times 10^{-4} \rightarrow 1.8 \times 10^{-3}$	-0.00078 $\rightarrow$ -0.00139
50 $\rightarrow$ 60	10.5	0.9681 $\rightarrow$ 0.9583	$12.7 \times 10^{-4} \rightarrow 1.7 \times 10^{-3}$	-0.00074 $\rightarrow$ -0.00129
50 $\rightarrow$ 60	10.6	0.9690 $\rightarrow$ 0.9598	$12.0 \times 10^{-4} \rightarrow 1.6 \times 10^{-3}$	-0.00070 $\rightarrow$ -0.00119
50 $\rightarrow$ 60	10.7	0.9698 $\rightarrow$ 0.9612	$11.8 \times 10^{-4} \rightarrow 1.5 \times 10^{-3}$	-0.00066 $\rightarrow$ -0.00111
50 $\rightarrow$ 60	10.8	0.9706 $\rightarrow$ 0.9626	$11.3 \times 10^{-4} \rightarrow 1.4 \times 10^{-3}$	-0.00062 $\rightarrow$ -0.00103
50 $\rightarrow$ 60	10.9	0.9714 $\rightarrow$ 0.9638	$10.9 \times 10^{-4} \rightarrow 1.4 \times 10^{-3}$	-0.00059 $\rightarrow$ -0.00096
50 $\rightarrow$ 60	11.0	0.9722 $\rightarrow$ 0.9650	$10.5 \times 10^{-4} \rightarrow 1.3 \times 10^{-3}$	-0.00056 $\rightarrow$ -0.00090
50 $\rightarrow$ 60	11.1	0.9729 $\rightarrow$ 0.9661	$10.1 \times 10^{-4} \rightarrow 1.2 \times 10^{-3}$	-0.00053 $\rightarrow$ -0.00084

range  $\beta \in [10.4, 11.1]$ . By determining the slow-roll parameters, we can compare the experimental data with the most suitable and optimal selections for each of the three free parameters in each of the three tables. This analysis allows us to extract extremely favorable outcomes. For the Figure 3, the values of  $r$  and  $n_s$  decrease with increasing  $\beta$  and fixing  $\mu$  and  $\alpha$ , and the value of  $n_s$  increases with increasing  $\beta$ .

As it was shown in the Figures 1–3, we have presented the correlation between the spectral indices  $r$  and  $n_s$ . Then, we compared the results, which were obtained from the slow-roll parameters, with the experimental data. They clearly yielded favorable results. It is important to note that all these implications and results are in the presence of our  $J(\phi)$ .

These behaviors are plotted in the Figures 1–3 by implementing the Planck line constraints [27], [28]. The values of the number of e-folds, which are established by the experimental values, belong to the interval  $N \in [50, 60]$ . Thus, the behaviors of the curve  $n_s - r$  with varying  $\alpha$ ,  $\beta$ , and  $\mu$  in the mentioned ranges are investigated.

When the scalar potential and scaled gravity are coupled with a kinetic term, it yields intriguing numerical values for  $n_s$  and  $r$ . These values fall within a favorable range of the

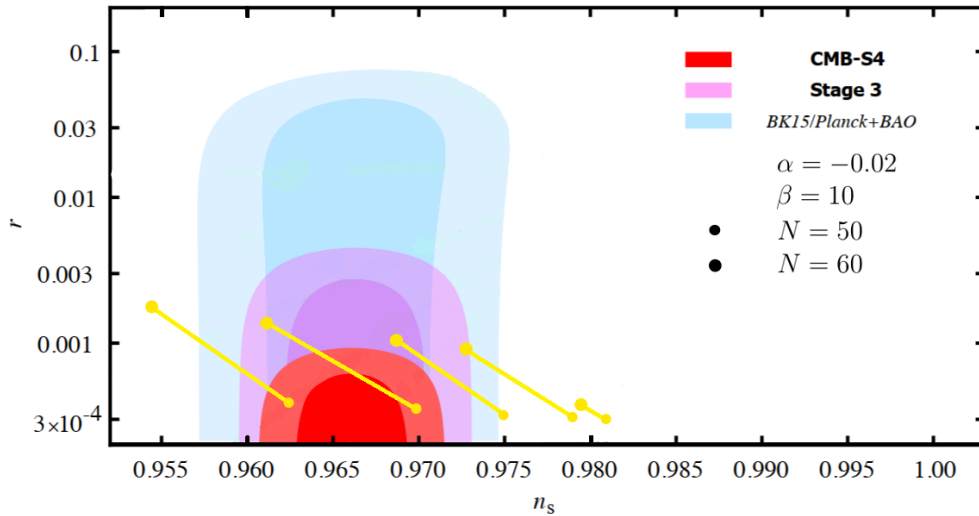


Figure 1: The tensor-to-scalar ratio  $r$  versus the scalar spectral index  $n_s$  for  $N = 50$ – $60$  e-folds. The solid lines show the model’s predictions for  $\alpha = -0.02$ ,  $\beta = 10$ ,  $p = 3$ , in which  $\mu$  varies in the range  $2.0 \leq \mu \leq 2.4$  (from top to bottom of the  $r$  values). The  $1\sigma$  and  $2\sigma$  confidence contours from the Planck 2018+BICEP/Keck 2018 data have been shown for comparison. For this parameter range, the model’s predictions fall well within the observational constraints.

Planck data, which includes both the 95% and 68% CL contour regions of the recently published BICEP/Keck data[27]-[29]. The Planck findings, which are smaller than 0.1, are in good agreement with the range of  $r$ , which is  $[6 \times 10^{-4}, 2 \times 10^{-3}]$ . It has been predicted that a kinetic term could be added to the coupling between the scalar potential and the scaled gravity [52], [57].

The Figures 4– 6 show the sensitivity plots of the parameters  $r$ ,  $n_s$  and  $\alpha_s$  with respect to the parameters  $\alpha$ ,  $\beta$  and  $\mu$ .

- Each subplot combines the theoretical predictions (blue curves) with the observational constraints (green bands) from the Planck 2018 data.

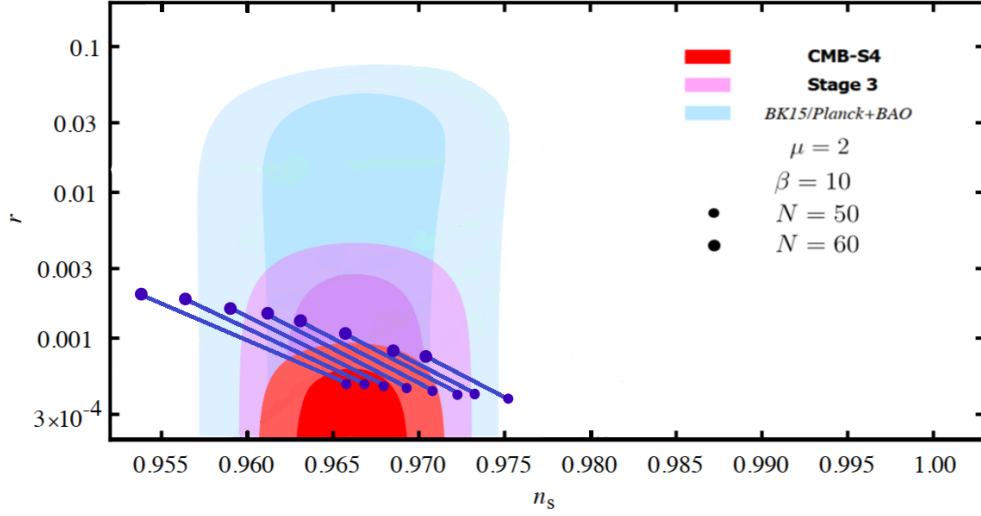


Figure 2: The tensor-to-scalar ratio  $r$  versus the scalar spectral index  $n_s$  for  $N = 50$ – $60$  e-folds. The solid lines show the model's predictions for  $\beta = 10$ ,  $\mu = 2$ ,  $p = 3$ , and  $\alpha$  varies in the range  $-0.21 \leq \alpha \leq -0.07$  (from top to bottom of the  $r$  values). The predictions have been plotted against the Planck 2018+BICEP/Keck 2018 confidence contours.

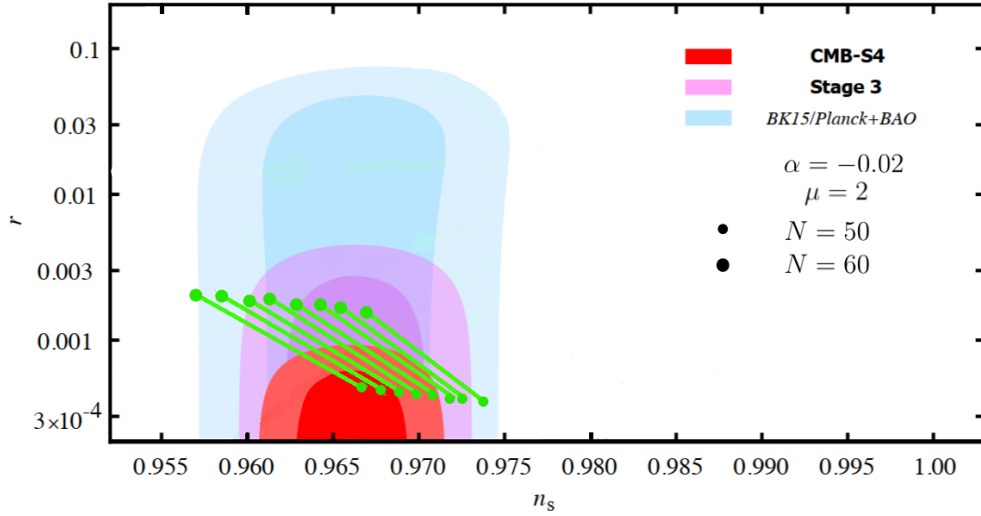


Figure 3: The tensor-to-scalar ratio  $r$  versus the scalar spectral index  $n_s$  for  $N = 50$ – $60$  e-folds. The solid lines show the model's predictions for  $\alpha = -0.02$ ,  $\mu = 2$ ,  $p = 3$ , and  $\beta$  varies in the range  $10.4 \leq \beta \leq 11.1$  (from top to bottom of the  $r$  values). The results are consistent with the observational bounds of the Planck 2018+BICEP/Keck 2018.

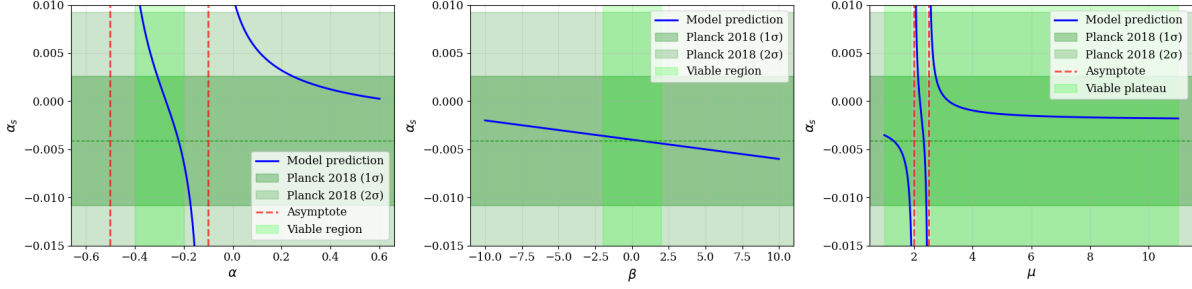


Figure 4: The parameter-space analysis of the running of the spectral index  $\alpha_s$  shows distinct functional dependencies. Left:  $\alpha_s(\alpha)$  exhibits asymptotic divergence at  $\alpha = -0.5$  and  $-0.1$ , which delineates the theoretical boundaries in the coupling parameter-space. Middle:  $\alpha_s$  linearly decreases with  $\beta$ , for the moderate  $\beta$  values, it remains within the Planck's  $2\sigma$  constraints. Right:  $\alpha_s(\mu)$  reveals a resonant structure with the singularities at  $\mu = 2.0$  and  $2.5$ , creating observationally viable plateaus in the intervening parameter regions. The theoretical prediction (the blue curve) has been evaluated against the observational constraints  $\alpha_s = -0.0041 \pm 0.0067$  from the Planck collaboration.

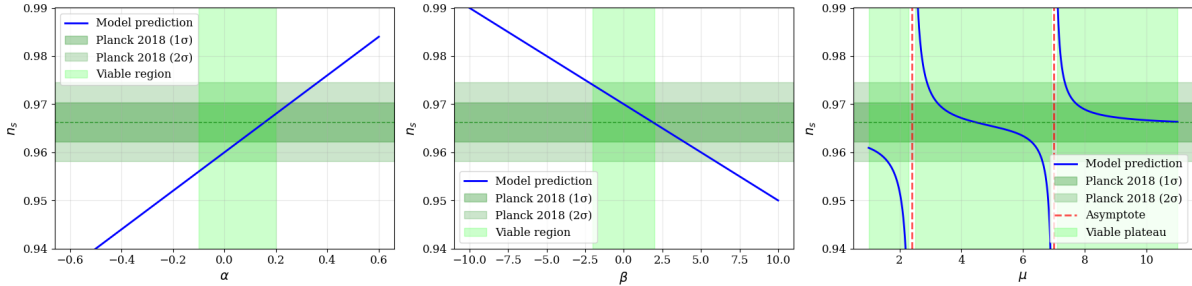


Figure 5: The sensitivity analysis of  $n_s$  across the fundamental inflationary parameters. Left:  $n_s(\alpha)$  monotonically increases with the coupling strength  $\alpha$ , which intersects the Planck preferred value  $n_s = 0.9663 \pm 0.0041$  at intermediate  $\alpha$  values. Middle:  $n_s(\beta)$  linearly decreases with the field parameter  $\beta$ ; the central values of  $\beta$  yield observationally consistent results. Right:  $n_s(\mu)$  features, separated by the asymptotes at  $\mu = 2.4$  and  $7.0$ , indicate the parameter regions where the spectral index remains stable against the mass scale variations. All viable regions (lemon) satisfy the observational constraints within the  $2\sigma$  confidence levels.

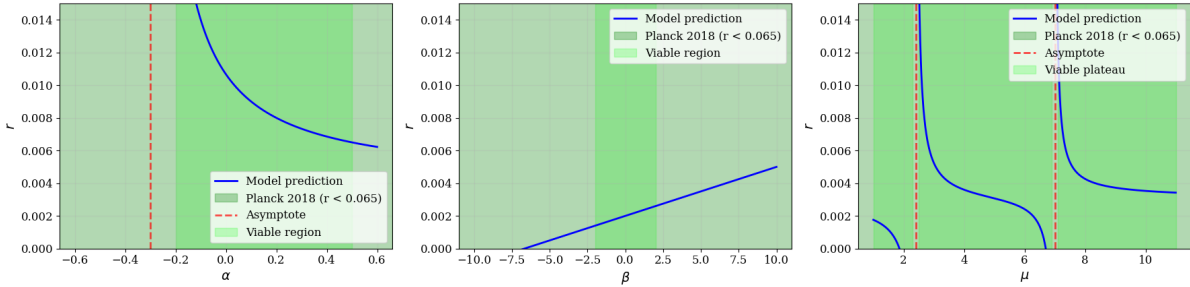


Figure 6: The dependence of  $r$  on the inflationary model parameters. Left:  $r(\alpha)$  displays a singular behavior at  $\alpha = -0.3$ , which indicates critical enhancement of the tensor mode generation. Middle:  $r(\beta)$  exhibits linear growth with the parameter  $\beta$ , which remains consistent with the Planck upper bound  $r < 0.065$  for  $\beta \lesssim 20$ . Right:  $r(\mu)$  shows resonant amplification near  $\mu = 2.4$  and  $7.0$ . The green-shaded region represents the observationally permitted parameter-space, where the viable inflationary trajectories occur when the theoretical predictions fall below the experimental limit.

- The vertical red-dashed lines indicate the theoretical asymptotes where the model predictions diverge.
- The colored backgrounds highlight the stable parameter regions, in which the lemon indicates the observationally viable zones.

The sensitivity analysis, presented in Figures 4–6, provides crucial insight into the viable parameter space of our model. The presence of the vertical asymptotes in these plots indicates the values of  $\alpha$ ,  $\beta$  and  $\mu$  where the denominators in the expressions for  $n_s$ ,  $r$  and  $\alpha_s$  vanish, leading to a divergence. These asymptotes are unphysical and represent a breakdown of the slow-roll approximation or an instability in the underlying theory for those specific parameter values. Consequently, the physically meaningful and observationally viable parameter-space is not located at these asymptotes, but rather in the stable regions between them. In these plateaus, the cosmological observables attain finite, nearly constant values that are robust against small variations in the parameters. The ranges for  $\alpha$ ,  $\beta$  and  $\mu$ , where they have been quoted in our analysis and they were used to generate the results in Tables 1–3 and the Figures 1–3, are chosen from within these stable regions. This demonstrates that the agreement with the Planck data is not a fine-tuned coincidence at a singular point, but is a robust prediction of the model across finite and well-defined intervals of its parameter-space.

## 3.2 Systematic analysis of the parameter space and naturalness

A principal result of this work is the identification of the regions in the model's parameter-space that yield predictions consistent with the latest cosmological constraints. To address this systematically, we have conducted a comprehensive numerical scan over the free parameters  $\alpha$ ,  $\beta$  and  $\mu$ , with the power  $p$  fixed to 3. This is for evaluating the resulting spectral index  $n_s$ , the tensor-to-scalar ratio  $r$  and the running  $\alpha_s$  for the cosmologically relevant range of  $N = 50$  to 60 e-folds.

The allowed ranges of the parameters, as rigorously determined by this scan and are summarized in the Tables 1–3, are:

- $\alpha \in [-0.21, -0.07]$
- $\beta \in [10.4, 11.1]$
- $\mu \in [2.0, 2.4] M_{\text{Pl}}$

These ranges are not isolated points but continuous intervals, which demonstrate that the agreement with the data is a robust prediction of the model and does not rely on the extreme fine-tuning. The corresponding observables fall within the following windows:

- $n_s \in [0.9485, 0.9817]$
- $r \in [0.0015, 0.007]$
- $\alpha_s \in [-0.00197, -0.00024]$

The question of the naturalness is paramount. The parameter  $\mu$ , which is of the order of the Planck mass  $M_{\text{Pl}}$ , is a natural scale for an effective field theory which describes the inflation. The parameters  $\alpha$  and  $\beta$ , which govern the strength and structure of the non-minimal kinetic coupling, are of the order  $\mathcal{O}(-0.02)$  and  $\mathcal{O}(10)$ , respectively. Crucially, they are not hierarchically large or small. That is, we do not require  $\beta/\alpha \sim 10^{10}$ . The values are technically natural in the sense that setting  $\alpha, \beta \rightarrow 0$  restores the standard GR limit, and the observed values are stable under small variations, as evidenced by the plateaus in the sensitivity plots (Figures 4– 6).

Besides, the model itself imposes a theoretical constraint that further informs the naturalness. As it will be detailed in the Conclusions section, the conditions  $\alpha \neq \pm\beta$  emerge from the requirement of a physically consistent slow-roll inflation and a graceful exit. The viable parameters ranges, that we have automatically identified, satisfy this theoretical prior. Therefore, the observationally allowed parameter space is not an arbitrary finely-tuned subset. It is meaningfully constrained by both theoretical consistency and experimental data. This synergy suggests that the presented parameter ranges are not only allowed but they are also theoretically preferred within the framework of our model.

## 4 Conclusions

We investigated the slow-roll dynamics corresponding to a scalar-tensor model that includes a non-minimal kinetic coupling. The potential is the DI and the coupling was represented as a power functional of the scalar field, characterized by two free parameters. In the context of the standard canonical scalar field, the DI potential yields significant solutions that characterize various phases of the cosmological development, which includes the accelerated expansion in the late universe. Besides, it provides solutions for the early-time inflation.

The spectral index  $n_s$  and  $r$  depend on the three free parameters  $\alpha$ ,  $\beta$  and  $\mu$ . When these parameters are quenched, the resulting values of  $n_s$  become inconsistent with the observational constraints. These parameters can be used to adjust the scalar field values at the end and at the beginning of the inflation. The  $n_s - r$  curves have been shown for the different cases. The Figures 1–3 were plotted for various values of  $\alpha$ ,  $\beta$  and  $\mu$ . Precisely, in each figure, two parameters have been fixed while the third parameter changes in a specified interval.

The model exhibits two specific limits. The first, when  $\alpha = -\beta$  and here is the  $\mu$  in the specified range  $[2, 2.4]$ . We derive  $n_s = 0.98140$  but  $r$  is incompatible with the Planck constraints. The second, when  $\alpha = \beta$ , with a specific and defined value for  $\mu \in [2, 2.4]$ , we obtain  $r = 0.0044$ , but the outcomes of  $n_s$  are inconsistent with the experimental data. Thus, for the physical consistency, these constraints necessarily impose  $\alpha \neq \pm\beta$ . Across

the cosmologically relevant range  $N \in [50, 60]$ , the model generates observationally viable parameters:  $r \in [0.0015, 0.007]$ ,  $n_s \in [0.9485, 0.9817]$  and  $\alpha_s \in [-0.00197, -0.00024]$ . The aforementioned results are consistent with the  $\alpha \neq \pm\beta$  conditions, otherwise, the slow rolling condition during the inflation and at the end of it would be violated.

The sensitivity diagrams of the quantities  $r$ ,  $n_s$  and  $\alpha_s$  versus the free parameters has been displayed. Our explanation revealed that the free parameters cannot take any arbitrary range. We found that  $n_s$ ,  $r$  and  $\alpha_s$  fall within the ranges that have been established by the most recent observational evidence. Actually, our sensitivity analysis reveals that the theoretical parameter-space is naturally segmented by asymptotes. The requirement for the cosmological observables  $n_s$ ,  $r$  and  $\alpha_s$  to be finite and stable directly restricts the parameters  $\alpha$ ,  $\beta$  and  $\mu$  to the plateaus between these asymptotic boundaries. The observationally viable ranges, that we have identified, are not arbitrarily chosen but they are a direct consequence of this underlying structure. The latter one inherently prevents the parameters from taking on unphysical values that would lead to divergences.

## References

- [1] A. H. Guth, Phys. Rev. **D 23** (1981) 347-356.
- [2] A. D. Linde, Phys. Lett. **B 108** (1982) 393.
- [3] H.P Nilles, Phys. Rep. **110** (1984) 1-162.
- [4] E. Witten, Nucl. Phys. **B 188** (1981) 513-554.
- [5] D. Baumann, L. McAllister, “*Inflation and String Theory. Cambridge University Press*”, 2015.
- [6] K.I Izawa, and T. Yanagida, Theor. Phys. **95** (1996) 829-830.
- [7] M. Arai, S. Kawai and N.Okada, Phys. Lett. **B 650** (2007) 133-138.
- [8] K. Nakayama, F. Takahashi and T.Watari, JHEP **12** (2011) 031.
- [9] A. H. Guth and P.J. Steinhardt, Scientific American **250** (1984) 129.

- [10] A. D. Linde, JETP Lett. **40** (1984) 1333.
- [11] A. Starobinsky, JETP Lett. **73** (2001) 371.
- [12] J. A. Adams, B. Cresswell and R. Easther, Phys. Rev. **D 64** (2001) 123514.
- [13] S. Nojiri, S. D. Odintsov and M. Sami, Phys. Rev. **D 74** (2006) 046004.
- [14] T. J Li, J. L. Lopez and D. V. Nanopoulos, Phys. Rev. **D 56** (1997) 2606.
- [15] M. Sami, N. Savchenko and A. Toporensky, Phys. Rev. **D 70** (2004) 123528.
- [16] X. Chen, R. Easther and E. A. Lim, JCAP **06** (2007) 023.
- [17] V. K. Oikonomou, Class. Quant. Grav. **38** (2021) 195025,
- [18] E. D. Stewart, Phys. Rev. **D 51** (1995) 684.
- [19] H. V. Peiris, D. Baumann, B. Friedman and A. Cooray, Phys. Rev. **D 76** (2007) 103517.
- [20] A. G. Cadavid and A. E. Romano, Eur. Phys. J. C **75** (2015) 589.
- [21] B. Li and J. D. Barrow, Phys. Rev. **D 75** (2007) 084010.
- [22] A. W. Beckwith, AIP Conf. Proc. **880** (2007) 1180.
- [23] V. F. Mukhanov and G. V. Chibisov, JETP Lett. **33** (1981) 532.
- [24] A. A. Starobinsky and H. J. Schmidt, Class. Quant. Grav. **4** (1987) 695.
- [25] J. M. Bardeen, Phys. Rev. **D 22** (1980) 1882.
- [26] J. M. Bardeen, P. J. Steinhardt and M. S. Turner, Phys. Rev. **D 28** (1983) 679.
- [27] Y. Akrami et al. “*Planck 2018 results. X. Constraints on inflation*”, Astron. Astrophys. **641** (2020) 10, [arXiv:1807.06211 [astro-ph.CO]].
- [28] N. Aghanim et al. “*Planck 2018 results. VI. Cosmological parameters*”, Astron. Astrophys. **641** (2020) 6, [arXiv:1807.06209 [astro-ph.CO]].

- [29] P. A. R. Ade et al. “*Improved Constraints on Primordial Gravitational Waves using Planck, WMAP, and BICEP/Keck Observations through the 2018 Observing Season*”, Phys. Rev. Lett. **127** (2021) 151301, [arXiv: 2110.00483 [astro-ph.CO]].
- [30] V. K. Oikonomou, Phys. Rev. **D 103** (2021) 044036; B. Li and J. D. Barrow, Phys. Rev. **D 75** (2007) 084010; S. Nojiri and S. D. Odintsov, Int. J. Geom. Meth. Mod. Phys. **4** (2007) 115; T. P. Sotiriou, V. Faraoni, Rev. Mod. Phys. **82** (2010) 451; A. De Felice, S. Tsujikawa, Living Rev. Rel. **13** (2010) 3.
- [31] K. Bamba, S. Nojiri, S. D. Odintsov and D. Sáez-Gómez, Phys. Rev. **D 90** (1983) 679; S. Tsujikawa, Lect. Notes Phys. **800** (2010) 99; S. Nojiri, S. D. Odintsov, Phys. Rept. **505** (2011) 59-144; S. Nojiri, S. D. Odintsov, V. K. Oikonomou, Phys. Rept. **692** (2017) 1-104.
- [32] H. Tiberiu, S. N. L. Francisco, N. Shin’ichi and S.D. Odintsov, Phys. Rev. **D 84** (2011) 024020; C. Germani and K. Kehagias, Phys. Rev. Lett. **105** (2010) 011302.
- [33] P. H. R. S. Moraes, J. D. V. Arbañil, and M. Malheiro, JCAP **06** (2016) 005.
- [34] F. Younesizadeh and D. Kamani, Gen. Rel. Grav. **57** (2025) 114, <https://doi.org/10.1007/s10714-025-03448-4>, arXiv:2507.23321 [gr-qc]; F. Younesizadeh and D. Kamani, Int. J. Theor. Phys. **64** (2025) 60, arXiv:2507.15812 [gr-qc]; J. Astrophys. Astr. **46** (2025) 42, arXiv:2507.19005 [gr-qc].
- [35] F. G. Alvarenga, A. dela Cruz-Dombriz, M. J. S. Houndjo, M. E. Rodrigues, and D. Sáez- Gómez, Phys. Rev. **D 87** (2013) 10.
- [36] S. Bhattacharjee, J. R. L. Santos, P. H. R. S. Moraes and P. K. Sahoo, Eur. Phys. J. Plus **137** (2020) 576.
- [37] W.H. Kinney and A. Riotto, Astropart. Phys. **10** (1999) 387.
- [38] W.H. Kinney and A. Riotto, Phys. Lett. **B 435** (1998) 272. K. Hamaguchi, K.L. Izawa, and H. Nakajima. Physics Letters **B 662** (2008) 208-12. I. Affleck, M. Dine and N. Seiberg. Nucl.Phys. **B 256** (1985) 557. K. Schmitz and T. T. Yanagida. Phys. Rev. **D 94** (2016) 074021.

- [39] G. W. Horndeski, *Int. J. Theor. Phys.* **10** (1974) 363–384.
- [40] T. Kobayashi, M. Yamaguchi, and J. Yokoyama, *Prog. Theor. Phys.* **126** (2011) 511–529.
- [41] D. J. Schwarz, C. A. Terrero-Escalante and A. A. Garca, *Phys. Lett. B* **517** (2001) 243; S. M. Leach et al. *Phys. Rev. D* **66** (2002) 023515.
- [42] A. Kosowski and M.S. Turner, *Phys. Rev. D* **52** (1995) 1739.
- [43] J. Martin and C. Ringeval, *JCAP* **08** (2006) 009.
- [44] A. Linde, *Phy. Rept.* **333-334** (2000) 575-591.
- [45] D. Baumann, [arXiv preprint, arXiv:0907.5424].
- [46] L. Kofman, A. Linde, and A.A. Starobinsky, *Phys. Rev. D* **56** (1997) 3258.
- [47] K. D. Lozanov and M. A. Amin, *Phys. Rev. D* **90**. 2014, 083528.
- [48] L. Boubekour and D. H. Lyth, *JCAP* **07** (2005) 010.
- [49] D. H. Lyth and A. Riotto, *Phy. Rept.* **314** (1999) 1-146.
- [50] J. Martin, C. Ringeval and V. Vennin. “*Encyclopaedia Inflationaris*”, *Phys. Dark Univ.* 5-6 (2014) 75-235 [arXiv: arXiv:1303.3787 [astro-ph.CO]].
- [51] N. A. Avdeev and A. V. Toporensky, *Gravitation and Cosmology* **28** (2022) 416; Q. Huang, H. Huang, F. Tu, L. Zhang and J. Chen, *Annals Phys.* **409** (2019) 167921; L. Wu, Q. Gao, Y. Gong, Y. Jia and T. Li, *Commun. Theor. Phys.* **73** (2021) 075402; S. Teymourtashlou and D. Kamani, *Eur. Phys. J. C* **81** (2021) 761, arXiv:2108.10164 [hep-th]; D. Kamani, *Phys. Lett. B* **564** (2003) 123-131, arXiv:hep-th/0304236 [hep-th].
- [52] N. A. Avdeev and A. V. Toporensky, *Gravitation and Cosmology* **27** (2021) 269; I. V. Fomin, S. V. Chervon and A. V. Tsyganov, *Eur. Phys. J. C* **80** (2020) 350; R. Fakir and W. G. Unruh, *Phys. Rev. D* **41** (1990) 1783-1791; Z. K. Guo and D. J.

- Schwarz, Phys. Rev. **D 81** (2010) 123520; H. Daniali and D. Kamani, Nucl. Phys. **B 975** (2022) 115683, arXiv:2202.09347 [hep-th].
- [53] Sebastian Belkner et al. “*CMB-S4: Iterative Internal Delensing and  $r$  Constraints*”, Astrophys. J. 964 (2024) 2, 148, [arXiv: 2310.06729 [astro-ph.CO]].
- [54] M. D. Niemack, “*Designs for a large- aperture telescope to map the CMB 10x faster,*”, Appl. Opt. **55** (2016) 1688-1696, [arXiv:1511.04506 [astro-ph.IM]].
- [55] T. Louis et al., “Atacama Cosmology Telescope DR6: Updated Constraints on Inflationary Parameters,” [arXiv:2503.14454 [astro-ph.CO]] (2025).
- [56] E. Calabrese et al., “ACT DR6: Cosmological Parameters with Planck and BAO,” [arXiv:2503.14452 [astro-ph.CO]] (2025).
- [57] S. Tsujikawa, Phys. Rev. **D 85** (2012) 083518.